GEOPHYSICAL RESEARCH LETTERS, VOL. 36, L03302, doi:10.1029/2008GL036560, 2009

Interseismic slip rate of the northwestern Xianshuihe fault from InSAR data

H. Wang,[1,2] T. J. Wright,[2] and J. Biggs[3]

Received 7 November 2008; revised 5 January 2009; accepted 8 January 2009; published 10 February 2009.

[1] The Xianshuihe fault is a highly active strike-slip fault system near the eastern margin of the Tibetan plateau. We use a multi-interferogram method to construct a map of line-of-sight deformation rate due to interseismic strain accumulation on the northwestern Xianshuihe fault from a decade of SAR data acquired by the ERS-1/2 and Envisat satellites. The rate map shows a clear deformation gradient associated with the fault, but slightly offset to the northeast from the surface trace. Joint inversion of InSAR rate map and GPS data using Monte-Carlo method, we estimate a slip rate of 9-12 mm/yr with a locking depth of 3-6 km at the 90% confidence level. The slip rate agrees with the Holocene fault slip rate and the historical earthquakes. Our results also suggest no significant across-fault extension. In the future, InSAR data from both ascending and descending orbits may further constrain the 3-D fault slip rate on this fault. **Citation:** Wang, H., T. J. Wright, and J. Biggs (2009), Interseismic slip rate of the northwestern Xianshuihe fault from InSAR data, *Geophys. Res. Lett.*, *36*, L03302, doi:10.1029/2008GL036560.

1. Introduction

[2] The ~350-km-long, left-lateral Xianshuihe fault in eastern Tibet (Figure 1) is a major intracontinental fault system in the Indo-Asian collision zone, on which over 20 $M > 6.5$ earthquakes have occurred since 1700 [*Division of Earthquake Monitoring and Prediction* (*DEMP*), 1995, 1999]. Understanding its present-day slip rate will better constrain geodynamic models, and aid the evaluation of its earthquake potential.

[3] Using field geological data, *Allen et al.* [1991] estimated a Holocene left-lateral slip rate that decreases from 15 ± 5 mm/yr at the northwest (NW) end to 5 mm/yr in the southeast (SE). *Xu et al.* [2003] re-estimated some sites and suggested rates of 14 ± 2 and 9.6 ± 1.7 mm/yr in the NW and SE respectively. *Wang et al.* [1998] estimated a total offset of ~60 km for 2–4 Ma, indicating an average long-term slip rate of 15–30 mm/yr. Recent GPS data suggest a slip rate of ~10 mm/yr along its whole length [e.g., *Shen et al.*, 2005; *Chen et al.*, 2000; *King et al.*, 1997].

[4] Interferometric synthetic aperture radar (InSAR) has been used for measuring interseismic deformation of the western or northern Tibetan plateau in a few studies [e.g., *Wright et al.*, 2004a; *Taylor and Peltzer*, 2006; *Jolivet et al.*, 2008; *Elliott et al.*, 2008]. Near the eastern margin, however, heavier vegetation coverage causes problems with decorrelation [*Zebker and Villasenor*, 1992], making conventional InSAR stacking approaches challenging. *Biggs et al.* [2007] proposed a multi-interferogram method for InSAR interseismic deformation analysis. The main advantages of this method are: (i) The orbital errors can be more efficiently corrected using an epoch-by-epoch network adjustment method, and (ii) the quantity of coherent points can be greatly increased using a pixel-by-pixel stacking strategy. *Elliott et al.* [2008] improved this method by also correcting interferograms for topographically-correlated atmospheric delay errors. In this study, we use this method to determine the interseismic slip of the NW Xianshuihe fault.

2. InSAR Data Analysis

[5] We use 23 radar images from the ERS-1/2 and Envisat satellites, acquired between 1996 and 2008 on descending track 376 (Figure 1). Interferograms are produced using the JPL/Caltech ROI_PAC software [*Rosen et al.*, 2004]. Topographic phase is removed using the Shuttle Radar Topography Mission 3-arcsecond DEM [*Farr and Kobrick*, 2000]. The interferometric coherence is highly variable, and somewhat unpredictable. In general, but not always, we find interferograms with perpendicular baselines less than 100 m, and those formed from images acquired in the same season to be most coherent. Following *Jónsson* [2008], coherence is further improved by multilooking, typically to 16 range looks, but occasionally to 32 or 64. Some interferograms have to be manually unwrapped by setting bridges between isolated coherent patches. We check the bridges and correct phase unwrapping errors using a phase closure technique [*Biggs et al.*, 2007]. In total 33 interferograms (18 ERS, 15 Envisat) are successfully unwrapped; 19 are selected that give the best coherence (Figure S1 of the auxiliary material[1]), and are subsampled to 360 m spacing. The interferograms cover a cumulative time interval of ~25 years.

[6] The multi-interferogram method uses an iterative algorithm with four steps: correction of orbital errors, correction of atmospheric delay errors, construction of a rate map, and estimation of the fault slip rate [*Biggs et al.*, 2007; *Elliott et al.*, 2008]. The best-fitting orbital errors in this study have slopes with a mean of zero and standard deviations of 0.31 (east) and 0.11 (north) mm/km, confirming a roughly normal distribution of these parameters [*Biggs*

[1]Department of Surveying Engineering, Guangdong University of Technology, Guangzhou, China.
[2]COMET, School of Earth and Environment, University of Leeds, Leeds, UK.
[3]Rosenstiel School of Marine and Atmospheric Science, University of Miami, Miami, Florida, USA.

0094-8276/09/2008GL036560$05.00

[1]Auxiliary materials are available in the HTML. doi:10.1029/2008GL036560.

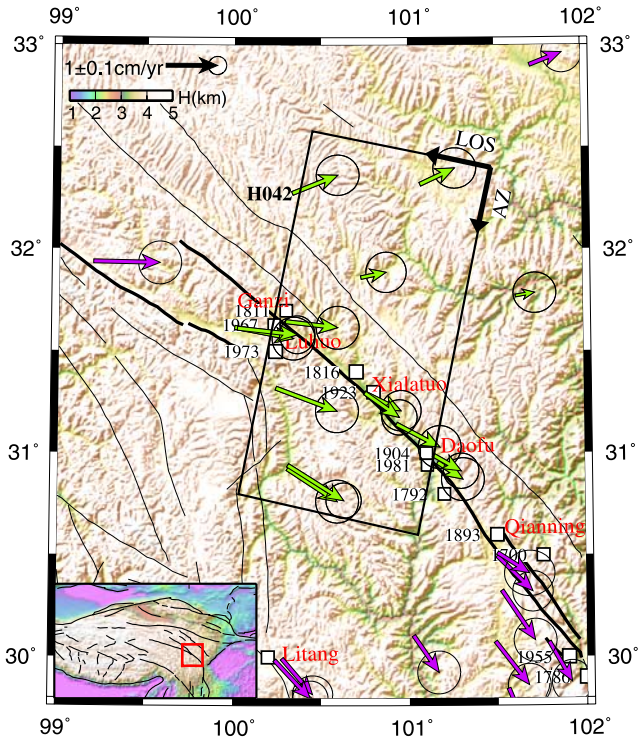

Figure 1. Topographic and tectonic map of the NW Xianshuihe area (inset shows the Tibetan plateau). The thick black lines indicate the Xianshuihe fault, and the thin lines show the other active or inactive faults. The black rectangle delimits the extents of our radar data. Two arrows on top of the rectangle show radar line-of-sight (LOS) and azimuth (AZ) directions respectively. The colored arrows are GPS velocities w.r.t South China block [*Shen et al.*, 2005], with those colored green being used in Figure 2. The small open squares denote historical earthquakes ($M > 6.5$) since 1700.

et al., 2007]. Atmospheric noise is modeled using an exponentially-decaying form of covariance function, yielding a mean e-folding wavelength of 10 km and variance of 20 mm^2. The wavelength agrees well with previous estimates of atmospheric noise [e.g., *Hanssen*, 2001; *Biggs et al.*, 2007], but the variance is smaller than that in Alaska [*Biggs et al.*, 2007], which is to be expected given the ~4 km average elevation. Topographically-correlated atmospheric delay errors are estimated and removed using a further network correction, assuming the delays vary linearly with height as a first-order approximation [*Elliott et al.*, 2008]. The estimates of the coefficients yield a mean value of zero with a standard deviation of 6 mm/km, smaller than obtained for the Altyn Tagh Fault [*Elliott et al.*, 2008]. A rate map is made by estimation of velocity on each pixel using an iterative least-squares algorithm with a full temporal covariance matrix. In this algorithm, the data point with the maximum residual is iteratively removed until the maximum residual is smaller than n (e.g., 3) times of the estimated atmospheric noise. The algorithm efficiently deletes outliers due to, in particular, phase unwrapping errors, thus derives a smoother rate map. Using this rate map at lower resolution (~3.6 km) and its full spatial covariance matrix, we solve for a final slip rate using a screw dislocation model [*Savage and Burford*, 1973], as well as the parameters for planar orbital and linear atmospheric corrections to cover the residuals of the first two steps. Figure 2 shows the LOS rate map and profile BB′ with the final orbital and atmospheric corrections removed. GPS data are also projected into local InSAR LOS directions, and the majority are consistent with InSAR observations showing a change in phase in a 20–30 km wide region across the fault. The strain zone is wider in the east than the west (Figure S2) suggesting a deeper locking depth there.

3. Slip Rate Inversion

[7] To explore the uncertainties of and covariances between slip rate and locking depth, we use a Monte-Carlo simulation of atmospheric delay errors [*Wright et al.*, 2003], synthesized using the statistics derived from real data, including spatial covariance. We estimate the slip rate and locking depth with GPS and InSAR data using a screw dislocation model [*Savage and Burford*, 1973]. We find that the estimates from the Monte-Carlo analysis are not dependent on the locking depth used in construction of the initial rate map. The parameter uncertainties are non-gaussian (Figures 3c and 3d), so we use confidence limits to describe them. Figure 3a shows that the horizontal velocities of 14 GPS stations alone (without H042) are not enough to determine locking depth, which ranges from 0 to 50 km (our upper limit). But GPS data give a slightly smaller slip rate than InSAR data for the same locking depth. The estimate from InSAR data is 10–16 mm/yr with a locking depth of 4–10 km at the 90% confidence level. This discrepancy may be due to the scarcity of GPS stations close to the fault or be because InSAR only measures a single component of the deformation field. We will test this in the future by determining horizontal and vertical motions directly using ascending and descending InSAR data [*Wright et al.*, 2004b], but insufficient ascending scenes are currently available. Joint inversion of GPS and InSAR data shows a better estimation of locking depth and slip rate. The slip rate estimate is 9–12 mm/yr with a locking depth of 3–6 km at the 90% confidence level, with the best-fit values of 11 mm/yr and 4 km. As found elsewhere [e.g., *Wright et al.*, 2001; *Taylor and Peltzer*, 2006; *Wallace et al.*, 2004], there is a strong trade-off between slip rate and locking depth, but this is reduced markedly with the joint inversion.

[8] Using block-like models, two recent studies suggest a large extension rate on the Xianshuihe fault (~8 mm/yr as given by *Thatcher* [2007] and 15 mm/yr by *Meade* [2007]), but both models have large residuals on this fault. We use the combined GPS and InSAR data to estimate the extension rate, as well as strike-slip rate and locking depth, using a buried tensile dislocation [*Okada*, 1985]. Our results give an extension rate of -0.5 ± 0.6 mm/yr implying no significant fault-normal motion (Figure S3), consistent with studies from GPS data alone [e.g., *Shen et al.*, 2005]. We assume no extension in the subsequent analyses.

4. Discussion

[9] Recent studies have reported asymmetric interseismic deformation from InSAR measurements on the Altyn Tagh [e.g., *Jolivet et al.*, 2008] and San Andreas faults [e.g., *Fialko*, 2006]. They invoked across-fault contrasts in the

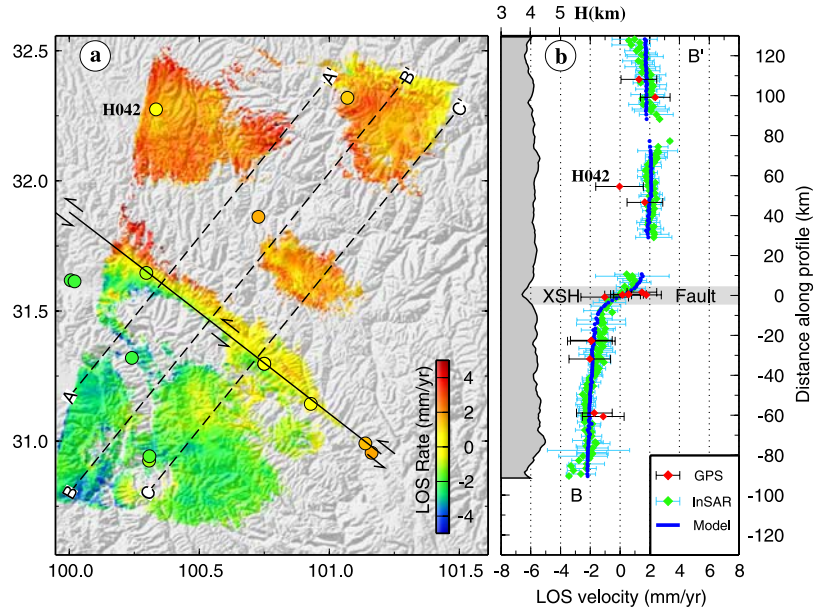

Figure 2. (a) LOS rate map stacked from 19 interferograms after removal of orbital and atmospheric delay errors. Colored circles indicate GPS velocities projected into the local LOS directions. The GPS values are also shifted by the average of all the GPS velocities to match the InSAR rate map. Positive values indicate motion away from satellite. A locking depth of 4 km is used in the iterative procedure that produces the rate map. (b) LOS InSAR (green), GPS (red) and model (blue) velocities, as well as topography (gray) along the profile BB′ (Figure 2a). The LOS velocity of each InSAR data point is calculated using the rates and their covariance matrix of all the pixels within a 1-km-wide bin along the profile. Horizontal bars denote the 2σ errors of the point measurements. The model results and GPS data are projected into the local InSAR LOS before producing the profile.

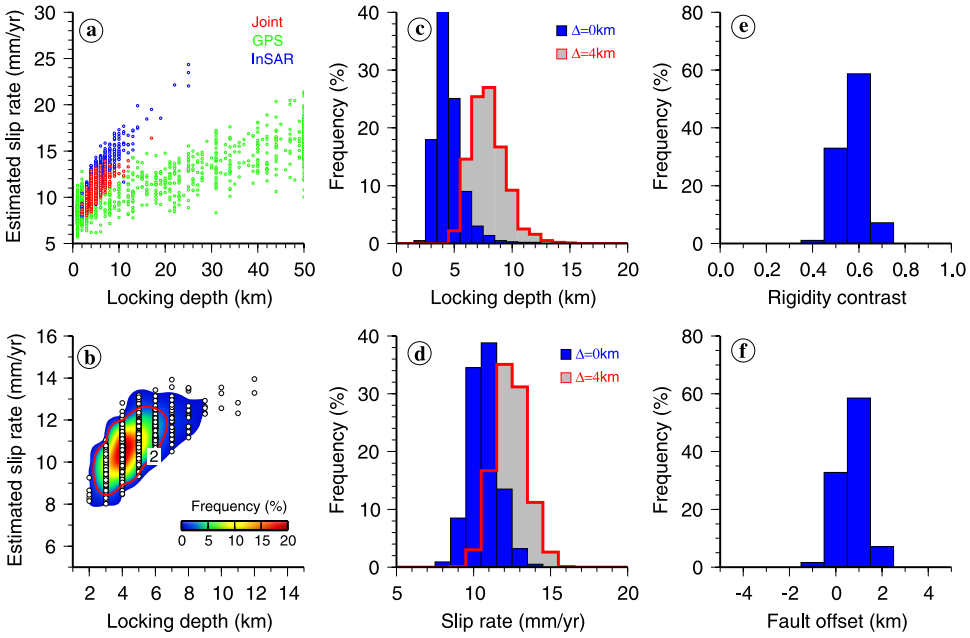

Figure 3. Fault parameters of the interseismic deformation model from 1000 data sets using a Monte-Carlo method. (a) Circles denote the best-fitting slip rate and locking depth for a screw dislocation model using GPS (green), InSAR (blue) and joint data (red). (b) Frequency contours of slip rate and locking depth for joint inversion. The frequencies are calculated by counting the number of the solutions on a regular grid (1 km by 1 mm). These are then smoothed and shown in color. The red contour indicates frequencies of 2%, which approximately enclose 90% of all the solutions. (c and d) Frequency of slip rate and locking depth from Monte-Carlo simulation. The blue and the gray histograms are obtained from a dislocation model with NE fault offset of 0 and 4 km respectively. (e and f) Frequency of across-fault rigidity contrast and fault offset for an asymmetric dislocation model with fixed locking depth of 4 km.

shear modulus (rigidity contrast, $K = \mu_2/(\mu_1 + \mu_2)$), and/or a horizontal offset between surface fault trace and the shear zone or dislocation at depth (fault offset, Δ). We incorporate K and Δ in a 2-D screw dislocation model to describe asymmetric surface velocity [*Jolivet et al.*, 2008], and use a Monte-Carlo method as above to find the best-fitting parameters. There is a strong trade-off between these two parameters. An optimal factor of $K = 0.6$ is obtained if fault location is fixed from the mapped traces (Figure 3e), implying that the rigidity of the host rocks on the SW side (μ_2) is about 1.5 times that of the NE (μ_1). Alternatively, the observations can be fit equally well by shifting the deep fault location ~1 km to the northeast (Figure 3f), implying a ~75° north-dipping fault plane assuming the mapped fault trace has been located correctly. We also find that northward fault offset gives larger values of locking depth and slip rate. For a fault offset of 4 km, the locking depth and slip rate are 8 km and 12 mm/yr respectively (Figures 3c and 3d). Discriminating between these models will only be possible using coseismic deformation in a future earthquake or with a microseismicity study of the fault.

[10] Independent estimates of locking depth for the Xianshuihe fault from seismic or geodetic data are not available because of the absence of large earthquakes since 1981, and previous studies usually analyzed the seismic data by fixing the depth [e.g., *Zhou et al.*, 1983a, 1983b]. The updated earthquake catalogue of *Jackson et al.* [2008] suggests centroid depths of 6–12 km from bodywave modeling for strike-slip earthquakes in Tibet. Geodetic modeling of the 1997 Manyi and the 2001 Kokoxili earthquakes indicate locking depths of about 10 km [e.g., *Peltzer et al.*, 1999; *Funning et al.*, 2007; *Lasserre et al.*, 2005]. There are few reliable estimates of locking depth for interseismic deformation in Tibet [e.g., *Wallace et al.*, 2004; *Taylor and Peltzer*, 2006]. The joint inversion in this study suggests a shallower locking depth than the observed in earthquakes. This could reflect a difference in behavior between interseismic and coseismic periods, or reflect the local geology around the Xianshuihe fault.

[11] Our result is consistent with the lower bound of the Holocene slip rate [*Allen et al.*, 1991; *Xu et al.*, 2003]. Since 1700, three large earthquakes have occurred on the 45-km-long Daofu segment (1792 M6.75, 1904 M7 and 1981 M6.9), and two on the 90-km-long Luhuo segment (1816 M7.5 and 1973 M7.6) (Figure 1). Earthquake recurrence intervals of ~75 and 150 years on these segments have been suggested [e.g., *Allen et al.*, 1991]. Assuming standard earthquake scaling relations for surface displacement to rupture length [*Wells and Coppersmith*, 1994], slip in the 1981 and the 1973 earthquakes was ~1 and ~2 m respectively. For our slip rate of 9–12 mm/yr, the earthquake recurrence intervals should be 83–110 and 166–220 years on the Daofu and Luhuo segments, consistent with historical earthquakes. For the 1981 Daofu earthquake, the empirical slip value of 1 m agrees well with the seismological result [*Zhou et al.*, 1983a]. For the 1973 Luhuo earthquake, *Zhou et al.* [1983b] obtained an average slip of 4 m with a fixed depth of 15 km, but the empirical value of 2 m is more consistent with our slip rate. Two earthquakes occurred in 1793 (M6.7) and 1893 (M7.3) on the ~62–km-long Qianning segment, southeast of our track. Assuming the slip rate on this segment is also 9–12 mm/yr implies an earthquake recurrence interval of 117–155 years. The earthquake probability on this segment is therefore very high, and likely to have been increased by the 2008 Sichuan earthquake [e.g., *Toda et al.*, 2008; *Parsons et al.*, 2008].

[12] **Acknowledgments.** This work is supported by the Royal Society through a Royal Society University Research Fellowship to TJW, and an International Incoming Fellowship to HW. HW is also supported by the Guangdong Natural Science Foundation (080094). The ERS and Envisat SAR data are copyrighted by the ESA, provided under projects Cat1-3392 and AOE-621. All the figures were prepared using the GMT software. We thank Barry Parsons, Alex Copley and Carolina Pagli for helpful discussions, and Fabio Florindo, Roland Bürgmann and two anonymous reviewers for comments that have improved the manuscript.

References

Allen, C. A., et al. (1991), Field study of a highly active fault zone: The Xianshuihe fault of southwestern China, *Geol. Soc. Am. Bull.*, *103*, 1178–1199.

Biggs, J., et al. (2007), Multi-interferogram method for measuring interseismic deformation: Denali fault, Alaska, *Geophys. J. Int.*, *170*, 1165–1179.

Chen, Z., et al. (2000), Global Positioning System measurements from eastern Tibet and their implications for India/Eurasia intercontinental deformation, *J. Geophys. Res.*, *105*, 16,215–16,227.

Division of Earthquake Monitoring and Prediction (DEMP) (1995), *Catalogue of Chinese Historical Strong Earthquakes* (in Chinese), Seismological, Beijing.

Division of Earthquake Monitoring and Prediction (DEMP) (1999), *Catalogue of Chinese Modern Earthquakes* (in Chinese), Sci. and Technol., Beijing.

Elliott, J. R., J. Biggs, B. Parsons, and T. J. Wright (2008), InSAR slip rate determination on the Altyn Tagh Fault, northern Tibet, in the presence of topographically correlated atmospheric delays, *Geophys. Res. Lett.*, *35*, L12309, doi:10.1029/2008GL033659.

Farr, M., and M. Kobrick (2000), Shuttle Radar Topography Mission produces a wealth of data, *Eos Trans. AGU*, *81*, 583–585.

Fialko, Y. (2006), Interseismic strain accumulation and the earthquake potential on the southern San Andreas fault system, *Nature*, *441*, 968–971.

Funning, G. J., B. Parsons, and T. J. Wright (2007), Fault slip in the 1997 Manyi, Tibet earthquake from linear elastic modelling of InSAR displacements, *Geophys. J. Int.*, *169*, 988–1008.

Hanssen, R. F. (2001), *Radar Interferometry: Data Interpretation and Error Analysis*, Kluwer Acad., Dordrecht, Netherlands.

Jackson, J., et al. (2008), New views on the structure and rheology of the lithosphere, *J. Geol. Soc. London*, *165*, 453–465.

Jolivet, R., R. Cattin, N. Chamot-Rooke, C. Lasserre, and G. Peltzer (2008), Thin-plate modeling of interseismic deformation and asymmetry across the Altyn Tagh fault zone, *Geophys. Res. Lett.*, *35*, L02309, doi:10.1029/2007GL031511.

Jónsson, S. (2008), Importance of post-seismic viscous relaxation in southern Iceland, *Nat. Geosci.*, *1*, 136–139.

King, R. W., et al. (1997), Geodetic measurement of crustal motion in southwest China, *Geology*, *25*, 179–182.

Lasserre, C., G. Peltzer, F. Cramp, Y. Klinger, J. Van der Woerd, and P. Tapponnier (2005), Coseismic deformation of the 2001 Mw = 7.8 Kokoxili earthquake in Tibet, measured by synthetic aperture radar interferometry, *J. Geophys. Res.*, *110*, B12408, doi:10.1029/2004JB003500.

Meade, B. J. (2007), Present-day kinematics at the India-Asia collision zone, *Geology*, *35*(1), 81–84.

Okada, Y. (1985), Surface deformation due to shear and tensile faults in a half-space, *Bull. Seismol. Soc. Am.*, *75*, 1135–1154.

Parsons, T., C. Ji, and E. Kirby (2008), Stress changes from the 2008 Wenchuan earthquake and increased hazard in the Sichuan basin, *Nature*, *454*, 509–510.

Peltzer, G., F. Crampé, and G. King (1999), Evidence of the nonlinear elasticity of the crust from *Mw*7.6 Manyi (Tibet) earthquake, *Science*, *286*, 272–276.

Rosen, P. A., S. Henley, G. Peltzer, and M. Simons (2004), Updated repeat orbit interferometry package released, *Eos Trans. AGU*, *85*(5), doi:10.1029/2004EO050004.

Savage, J. C., and R. O. Burford (1973), Geodetic determination of relative plate motion in central California, *J. Geophys. Res.*, *78*, 832–845.

Shen, Z.-K., J. Lü, M. Wang, and R. Bürgmann (2005), Contemporary crustal deformation around the southeast borderland of the Tibetan Plateau, *J. Geophys. Res.*, *110*, B11409, doi:10.1029/2004JB003421.

Taylor, M., and G. Peltzer (2006), Current slip rates on conjugate strike-slip faults in central Tibet using synthetic aperture radar interferometry, *J. Geophys. Res.*, *111*, B12402, doi:10.1029/2005JB004014.

Thatcher, W. (2007), Microplate model for the present-day deformation of Tibet, *J. Geophys. Res.*, *112*, B01401, doi:10.1029/2005JB004244.

Toda, S., J. Lin, M. Meghraoui, and R. S. Stein (2008), 12 May 2008 M = 7.9 Wenchuan, China, earthquake calculated to increase failure stress and seismicity rate on three major fault systems, *Geophys. Res. Lett.*, *35*, L17305, doi:10.1029/2008GL034903.

Wallace, K., G. Yin, and R. Bilham (2004), Inescapable slow slip on the Altyn Tagh fault, *Geophys. Res. Lett.*, *31*, L09613, doi:10.1029/2004GL019724.

Wang, E., et al. (1998), The Cenozoic Xianshuihe-Xiaojiang, Red River, and Dali fault systems of southwestern Sichuan and central Yunnan, China, *Geol. Soc. Am. Spec. Pap.*, *327*, 1–108.

Wells, D. L., and K. J. Coppersmith (1994), New empirical relationships among magnitude, rupture length, rupture width, rupture area and surface displacement, *Bull. Seismol. Soc. Am.*, *84*, 974–1002.

Wright, T., B. Parsons, and E. Fielding (2001), Measurement of interseismic strain accumulation across the North Anatolian Fault by satellite radar interferometry, *Geophys. Res. Lett.*, *28*, 2117–2120.

Wright, T. J., Z. Lu, and C. Wicks (2003), Source model for the M w 6.7, 23 October 2002, Nenana Mountain Earthquake (Alaska) from InSAR, *Geophys. Res. Lett.*, *30*(18), 1974, doi:10.1029/2003GL018014.

Wright, T. J., et al. (2004a), InSAR observations of low slip rates on the major faults of western Tibet, *Science*, *305*, 236–239.

Wright, T. J., B. E. Parsons, and Z. Lu (2004b), Toward mapping surface deformation in three dimensions using InSAR, *Geophys. Res. Lett.*, *31*, L01607, doi:10.1029/2003GL018827.

Xu, X., et al. (2003), Pattern of latest tectonic motion and its dynamics for active blocks in Sichuan-Yunnan region, China (in Chinese), *Sci. China*, *33*(z1), 151–162.

Zebker, H. A., and J. Villasenor (1992), Decorrelation in interferometric radar echoes, *IEEE Trans. Geosci. Remote Sens.*, *30*, 950–959.

Zhou, H.-L., H.-L. Liu, and H. Kanamori (1983a), Source processes of large earthquakes along the Xianshuihe fault in southwestern China, *Bull. Seismol. Soc. Am.*, *73*, 537–551.

Zhou, H.-L., C. R. Allen, and H. Kanamori (1983b), Rupture complexity of the 1970 Tonghai and 1973 Luhuo earthquakes, China, from P-Wave inversion, and relationship to surface faulting, *Bull. Seismol. Soc. Am.*, *73*, 1585–1597.

J. Biggs, Rosenstiel School of Marine and Atmospheric Science, University of Miami, 4600 Rickenbacker Causeway, Miami, FL 22149, USA. (jbiggs@rsmas.miami.edu)

H. Wang, Department of Surveying Engineering, Guangdong University of Technology, Guangzhou, Guangdong 510006, China. (ehwang@163.com)

T. J. Wright, COMET, School of Earth and Environment, University of Leeds, Leeds LS2 9JT, UK. (t.wright@see.leeds.ac.uk)